

This discussion paper is/has been under review for the journal Geoscientific Model Development (GMD). Please refer to the corresponding final paper in GMD if available.

High resolution land surface fluxes from satellite data (HOLAPS v1.0): evaluation and uncertainty assessment

A. Loew^{1,2}, J. Peng², and M. Borsche³

¹Ludwig-Maximilians Universität München, Luisenstr. 37, 80333 Munich, Germany

²Max Planck Institute for Meteorology, Bundesstr. 53, 20146 Hamburg, Germany

³Deutscher Wetterdienst, National Climate Monitoring, Frankfurter Str. 135, 63067 Offenbach, Germany

Received: 8 December 2015 – Accepted: 16 December 2015 – Published: 21 December 2015

Correspondence to: A. Loew (alexander.loew@lmu.de)

Published by Copernicus Publications on behalf of the European Geosciences Union.

GMDD

8, 10783–10841, 2015

High resolution land surface fluxes from satellite data (HOLAPS v1.0)

A. Loew et al.

Title Page

Abstract

Introduction

Conclusions

References

Tables

Figures

◀

▶

◀

▶

Back

Close

Full Screen / Esc

Printer-friendly Version

Interactive Discussion



Abstract

Surface water and energy fluxes are essential components of the Earth system. Surface latent heat fluxes provide major energy input to the atmosphere. Despite the importance of these fluxes, state-of-the-art datasets of surface energy and water fluxes largely differ. The present paper introduces a new framework for the estimation of surface energy and water fluxes at the land surface, which allows for temporally and spatially high resolved flux estimates at the global scale (HOLAPS). The framework maximizes the usage of existing long-term satellite data records and ensures internally consistent estimates of the surface radiation and water fluxes. The manuscript introduces the technical details of the developed framework and provides results of a comprehensive sensitivity and evaluation study. Overall the results indicate very good agreement with in situ observations when compared against 49 FLUXNET stations worldwide. Largest uncertainties of latent heat flux and net radiation were found to result from uncertainties in the global solar radiation flux obtained from satellite data products.

1 Introduction

Water and energy fluxes between the land surface and atmosphere are essential components of the Earth system. In the last years land-atmosphere fluxes have been mainly measured locally at the ecosystem scale by a network of flux tower sites within the frame of FLUXNET (Baldocchi, 2008; Baldocchi et al., 2001). However, to generate global datasets of water and energy fluxes, the use of satellite data as well as models has become indispensable.

Different approaches exist to infer land turbulent surface fluxes by either one of the following methods (Kalma et al., 2008; Wang and Dickinson, 2012): (1) simulations by an off-line land surface model (Roads and Betts, 2000); (2) empirical statistical models, like e.g. obtained by machine learning techniques or neural networks (Jung et al.,

High resolution land surface fluxes from satellite data (HOLAPS v1.0)

A. Loew et al.

Title Page

Abstract

Introduction

Conclusions

References

Tables

Figures



Back

Close

Full Screen / Esc

Printer-friendly Version

Interactive Discussion



is based on a state-of-the-art land surface scheme. HOLAPS allows for the estimation of surface energy and water fluxes at high temporal (< 1 h) and spatial (~ 5 km) resolutions. The required drivers for HOLAPS comprise satellite data at different processing levels as well as re-analysis data for a limited number of variables.

The objectives of the present study are mainly twofold. First, we introduce and validate the surface fluxes from the novel HOLAPS framework at global scales. Second, we perform a thorough uncertainty assessment of the impact of different forcing datasets on the accuracy of surface flux estimates. The latter is motivated by the question how much uncertainty is introduced when using globally available satellite information as a driver for land surface models compared to local data. The HOLAPS results are validated using tower based eddy-covariance measurements for a wide range of ecosystems and climates.

We first briefly introduce the HOLAPS concept and framework in Sect. 2. The datasets and methods are introduced in Sects. 3 and 4 respectively. Results and conclusions summarize the study.

2 Model

The High resOlution Land Atmosphere Parameters from Space (HOLAPS v1.0) framework is used for the estimation of global surface water and energy fluxes. It is based on a state of the art land surface model and was in particular designed to maximize the usage of satellite data as drivers as well as to ensure internal consistency of the different energy and water fluxes. HOLAPS is used for the estimation of global surface fluxes at high spatial and temporal resolutions. Figure 1 gives an example of HOLAPS long-term mean latent heat flux estimates for the global scale with a spatial resolution of 5 km.

Figure 2 shows the general surface state and fluxes simulated by HOLAPS. The all sky surface solar irradiance $S^{\downarrow} \text{ W m}^{-2}$ is either obtained from remote sensing products or is calculated internally by the HOLAPS radiation module using the MAGIC

GMDD

8, 10783–10841, 2015

High resolution land surface fluxes from satellite data (HOLAPS v1.0)

A. Loew et al.

Title Page

Abstract

Introduction

Conclusions

References

Tables

Figures



Back

Close

Full Screen / Esc

Printer-friendly Version

Interactive Discussion



High resolution land surface fluxes from satellite data (HOLAPS v1.0)A. Loew et al.

[Title Page](#)[Abstract](#)[Introduction](#)[Conclusions](#)[References](#)[Tables](#)[Figures](#)[◀](#)[▶](#)[◀](#)[▶](#)[Back](#)[Close](#)[Full Screen / Esc](#)[Printer-friendly Version](#)[Interactive Discussion](#)

radiative transfer model (Mueller et al., 2009). The algorithm requires information on aerosol properties, surface albedo (α) as well as total column water vapor content (TCW) kg m^{-2} . Aerosol properties are taken from an aerosol climatology (Kinne et al., 2013). Total column water vapor content can be either derived from climatologies or re-analysis data. Details on the accuracy of the MAGIC radiative transfer model is provided by Posselt et al. (2012).

The land surface scheme is explicitly coupled to a 1-D mixed layer for the planetary boundary layer (PBL) which is used to calculate the surface downwelling radiation consistently with the surface heat fluxes. As the PBL temperature and height are directly linked to the surface turbulent fluxes, a combination of the surface heat fluxes with a PBL model helps to better constrain the surface heat flux estimates (Anderson et al., 2007; Margulis and Entekhabi, 2001). A mixed boundary layer model is assumed (Kim and Entekhabi, 1998; Margulis and Entekhabi, 2001; Smeda, 1979).

The surface water fluxes comprise vegetation interception, soil moisture dynamics as well as evaporation and transpiration processes. The soil moisture dynamics is explicitly simulated using a discretization in different soil layers. The soil moisture information is used e.g. for the estimation of the surface resistance to evapotranspiration.

The present paper will focus exclusively on the validation of HOLAPS 1.0 results using in-situ flux tower measurements as well as the assessment of the sensitivity of HOLAPS to forcing perturbations. An assessment of spatiotemporal dynamics estimated from HOLAPS and cross comparison against other existing global datasets like e.g. the LandFlux-EVAL dataset (Mueller et al., 2013) will be performed in a separate study.

All symbols are summarized in Appendix A. Details for the entire model formulation are provided in Appendix B.

policies. For the present study we only use data from stations, which provide their data under a “Free Fair Use” license (<http://www.fluxdata.org>).

Eddy covariance measurements are subject to uncertainties from various sources. A common problem is that the eddy-covariance measurements typically do not allow to close the surface energy balance ($R_N - G - H - LE = 0$). The energy imbalance for eddy covariance measurements can be as high as 20 to 30 % on average (e.g. Wilson et al., 2002). The reason for this energy balance closure problem is still not fully understood and subject of ongoing research (e.g. Ingwersen et al., 2015). Several approaches have been developed to empirically correct for the energy closure (Foken et al., 2011; Ingwersen et al., 2015; Twine et al., 2000; Wilson et al., 2002). A simple energy balance correction is applied in this study following the approach as described in Twine et al. (2000). Further uncertainties in the FLUXNET data occur under stable conditions. As the eddy covariance method requires turbulent conditions (Berbigier et al., 2001).

3.2 Large scale forcing data

In the following we will briefly summarize the different forcing datasets used within HO-LAPS. Only dataset available at global scale are used and their details are summarized in Table 1.

3.2.1 Radiation data

The surface solar radiation flux (S^\downarrow) is either prescribed from existing satellite data products or can be calculated internally within the HOLAPS framework (cf. Appendix B2.2). In both cases a maximum consistency between the shortwave and longwave radiation fluxes is ensured as the same ancillary data (TCW, cloud fractional coverage) is used. This explicit internal consistency of the radiation flux estimates is unique to the HOLAPS framework.

GMDD

8, 10783–10841, 2015

High resolution land surface fluxes from satellite data (HOLAPS v1.0)

A. Loew et al.

Title Page

Abstract

Introduction

Conclusions

References

Tables

Figures

◀

▶

◀

▶

Back

Close

Full Screen / Esc

Printer-friendly Version

Interactive Discussion



As the surface solar radiation is a major input to the surface energy balance, it is expected that uncertainties in radiation data will also affect the accuracy of the derived water and energy fluxes.

Different approaches to estimate S^{\downarrow} are therefore analyzed in the present study. The following radiation datasets are used:

- *FLUXNET*: The radiation data measured at each FLUXNET station is used as a reference as these local measurements are expected to provide the most accurate surface solar radiation estimates for the FLUXNET locations. They capture also local changes in S^{\downarrow} at high temporal frequencies (e.g. cloud shadowing) and might also be affected by local effects like topographic conditions.
- *CM SAF-SIS*: The EUMETSAT Climate Monitoring Satellite Application Facility (CM-SAF) has specialized in the generation of long-term climate data records from satellite. As part of their suite of radiation data products (www.cmsaf.eu), the CM SAF provides solar incoming surface radiation (SIS) data at hourly timescales and with a spatial resolution of 0.03° (Posselt et al., 2012) for all sky conditions. The CM SAF-SIS is based on data from the series of METEOSAT satellites. It therefore provides only a limited area coverage (see Fig. 3).
- *GRIDSAT*: The Gridded Satellite dataset (GRIDSAT) (Knapp et al., 2011) provides a long-term (January 1980 to present) record of top-of-atmosphere (TOA) radiances in the visible and thermal spectral domains. It is based on the International Satellite Cloud Climate Project (ISCCP) (Knapp, 2008; Rossow and Schiffer, 1991) and provides data every 3-h on an equal angular grid with a resolution of $\sim 0.07^{\circ}$.

These TOA radiances in the visible channels are used to estimate a cloud effective albedo (CAL) (Posselt et al., 2012) which is then used subsequently for the calculation of S^{\downarrow} and cloud cover fraction (cf. Sect. B2.2).

High resolution land surface fluxes from satellite data (HOLAPS v1.0)

A. Loew et al.

Title Page

Abstract

Introduction

Conclusions

References

Tables

Figures



Back

Close

Full Screen / Esc

Printer-friendly Version

Interactive Discussion



3.2.2 Precipitation data

Satellite precipitation datasets are produced from satellite only or combined satellite and ground based measurements at a variety of spatial (0.25 to 2°) and temporal (3-hourly to monthly) resolutions at the global scale. Ground based precipitation estimates like e.g. from ground based rain radars provide even higher temporal and spatial resolution, but are available only for limited areas. A comprehensive review and inter-comparison of existing satellite based precipitation products and their application is provided by Kidd et al. (2012) and Kucera et al. (2013)

The TRMM Multisatellite Precipitation Analysis (TMPA) product (3B42 v7) is used for the present study (Huffman et al., 2007). It combines microwave sounding and infrared observations and compensates product biases using rain gauge information on monthly timescales. TMPA provides 3-hourly precipitation information at a spatial resolution of 0.25°. It is available since 1998 until present and covers the geographical extent of 50° N to 50° S.

The high temporal frequency of the measurements is a major advantage for flux estimates and the main reason why TMPA is currently used within HOLAPS. The spatial extent of TMPA however currently limits the application of HOLAPS to that same extent ($\pm 50^\circ$ latitude).

3.2.3 Vegetation data

Leaf area index (LAI) data products from the Moderate Resolution Spectroradiometer (MODIS) instruments (Justice et al., 2002) are used in the present study. We use an enhanced product from Beijing Normal University¹ (Yuan et al., 2011) which provides enhanced temporal and spatial consistency of the MODIS LAI fields by post-processing the original MOD15A2 products (Myneni et al., 2002). This results in much more con-

¹<http://globalchange.bnu.edu.cn/research/lai>

GMDD

8, 10783–10841, 2015

High resolution land surface fluxes from satellite data (HOLAPS v1.0)

A. Loew et al.

Title Page

Abstract

Introduction

Conclusions

References

Tables

Figures



Back

Close

Full Screen / Esc

Printer-friendly Version

Interactive Discussion



sistent LAI fields than in the original product which contains abrupt changes in the time series.

Surface albedo information is obtained from the ESA GlobAlbedo project (Muller et al., 2012; Potts et al., 2013).

Both, LAI data and surface albedo are available every 8-days. As both variables are varying slowly in time, they are linearly interpolated to the model timestep.

3.2.4 Re-analysis data

A limited number of additional fields (temperature, wind speed, total column water vapor path, pressure) are required from global re-analysis as these variables are not available from remote sensing data at the required temporal and spatial scales. The ERA-interim re-analysis (Dee et al., 2011) fields are used for that purpose which provide 6-hourly data on a regular global grid with 512 times 256 grid points, which corresponds to a spatial sampling of $\sim 0.7^\circ$. The re-analysis fields are remapped to the flux tower locations using bilinear interpolation.

3.2.5 Landcover data

Global landcover information is available with a spatial resolution of 300 m from the ESA Climate Change Initiative landcover project (Bontemps et al., 2012; Defourny et al., 2014). The land cover information is used for the spatial discretization of land cover dependent parameters in HOLAPS like e.g. roughness length or surface resistance parameters. These are summarized in Table B1.

However for the present study, no global landcover dataset is used as the experiments conducted are only performed on the point scale. The landcover type is known for each FLUXNET station and is therefore used in the present study.

GMDD

8, 10783–10841, 2015

High resolution land surface fluxes from satellite data (HOLAPS v1.0)

A. Loew et al.

Title Page

Abstract

Introduction

Conclusions

References

Tables

Figures



Back

Close

Full Screen / Esc

Printer-friendly Version

Interactive Discussion



3.2.6 Soil data

Information on soil properties is obtained from the Harmonized World Soil Database (HWSD) (FAO, 2012). Currently the HWSD is the only globally available soil information. The HWSD is based on soil mapping units with varying sizes. Thus no fixed resolution can be given, but the map is gridded with a spatial spacing of 30 arcsec. The information on soil texture (sand, clay content) is used to derive soil hydrological properties using pedo-transfer functions (Cosby et al., 1984; Lee, 2005; Rawls and Brakensiek, 1985).

As the HWSD is a global dataset, the local soil properties might differ from the one of the used mapping units. Further uncertainties are introduced by the applied pedo-transfer functions (e.g. Wösten et al., 2001).

4 Methods

4.1 Experimental setup

To quantify the accuracy of HOLAPS and the uncertainties related to the usage of satellite data as drivers we conduct a series of sensitivity experiments. Using the different datasets introduced in Sect. 3.2, we aim to investigate the uncertainty introduced by replacing a locally measured forcing with satellite based drivers. First a control simulation (CTRL) is conducted which is based exclusively on local measurements from FLUXNET only. This allows to quantify HOLAPS accuracies without additional uncertainties from the driver variables. Thus, the CTRL simulation is considered as the baseline accuracy of the current HOLAPS framework. For each site multiple years are used for the simulations (see Table 2). Results are then compared against reference measurements from FLUXNET and the accuracy of the simulations is quantified using various skill scores (cf. Sect. 4.2.1).

4.2 Analysis

We compare the net radiation and latent heat flux of HOLAPS with the corresponding reference data from FLUXNET at hourly, daily and monthly timescales using standard statistical skill scores. The variance of the difference between the model simulations and FLUXNET data is a function of (a) the uncertainties of the HOLAPS model itself, (b) the sensitivity of the HOLAPS model to uncertainties in the forcing data as well as (c) uncertainties in the FLUXNET reference data. Uncertainties in the FLUXNET measurements might also result from varying temporal and spatial footprints of the flux tower measurements (Chen et al., 2011).

4.2.1 Statistical metrics

The mean squared difference E^2 between in situ observations (x) and model results (y) is given as

$$E^2 = \frac{1}{N} \sum_i^N (x_i - y_i)^2 = \bar{E}^2 + E'^2 = \text{RMSD}^2 \quad (1)$$

with the bias $\bar{E} = \bar{x} - \bar{y}$. The overbar indicates temporal averaging. The root mean square difference (RMSD) is defined as the square root of Eq. (1). For the calculation of the centered root mean square difference (cRMSD), the bias is removed in advance. It is then defined as

$$E' = \sqrt{\frac{1}{N} \sum_{i=1}^N [(x_i - \bar{x}) - (y_i - \bar{y})]^2} = \text{cRMSD} \quad (2)$$

which is related to the Pearson correlation coefficient (r) as (Taylor, 2001)

$$E'^2 = \sigma_x^2 + \sigma_y^2 - 2\sigma_x\sigma_y r \quad (3)$$

daily and monthly flux estimates for the CTRL_G simulations. The correlation coefficient ranges between $r = 0.86$ for hourly data to $r = 0.78$ for daily and monthly data.

Error statistics for all experiments is provided in Fig. 8. The increased uncertainty in the surface solar radiation and thus R_N has a direct effect on the accuracy of the latent heat flux estimates. Correlation coefficients are smallest for the experiments that use satellite surface solar radiation data. However, the correlations are still high with $r > 0.7$ for most of the stations and experiments. The RMSD for the CTRL simulations ranges between 37 and 58 W m^{-2} for the majority of the cases. Largest RMSD is observed for the METEOSAT and GRIDSAT experiments. However, results from the experiments when replacing the air temperature and wind speed with re-analysis data show that this introduces also uncertainties in the latent heat flux estimates. The RMSD ranges between 40 and 62 W m^{-2} for these experiments. Corresponding results for daily and monthly timescales are provided in Figs. D3 and D4.

5.4 Summary of HOLAPS accuracies

So far we have summarized the overall accuracies of HOLAPS for the different experiments. As the HOLAPS framework is designed to be used at the global scale with a maximum of satellite and re-analysis data as drivers, we summarize in the following the accuracy of the HOLAPS results for the GRIDSAT_G experiment which corresponds to the case where only satellite and re-analysis drivers are used for HOLAPS flux estimates. Results are compared against the accuracy of the CTRL_G experiment that uses exclusively FLUXNET station data and the same stations. The overall accuracies at hourly, daily and monthly timescales for these two experiments are summarized in Table 3.

On monthly timescales, the results for the latent heat flux of the CTRL simulations and GRIDSAT based estimates are rather comparable. The correlation is $r = 0.75$ and $r = 0.78$ and RMSD are 30.1 and 30.2 W m^{-2} for the GRIDSAT_G and CTRL_G experiments respectively. However at the hourly and daily timescales the RMSD can be 20–

GMDD

8, 10783–10841, 2015

High resolution land surface fluxes from satellite data (HOLAPS v1.0)

A. Loew et al.

Title Page

Abstract

Introduction

Conclusions

References

Tables

Figures

⏪

⏩

◀

▶

Back

Close

Full Screen / Esc

Printer-friendly Version

Interactive Discussion



reported by Müller et al. (2015) where the daily RMSD of the product is reported to be 17.9 W m^{-2} . Thus, further investigations are required to investigate the results obtained in this study. As a further improvement of the surface solar radiation flux is expected to improve the latent heat flux estimates, a further thorough investigation of the impact of different surface solar radiation dataset will be performed in a future study.

7 Conclusions

This study has introduced a new framework for the estimation of high resolution land surface water and energy fluxes, HOLAPS. The framework was developed to maximize the usage of existing satellite data records and to allow for the generation of temporal and spatial high resolved and consistent global water and energy fluxes. This first study analyzed the accuracy of HOLAPS using data from 49 eddy covariance towers. A sensitivity analysis was performed to investigate the tradeoff in using satellite data as drivers instead of locally measured tower based data. The accuracy of the HOLAPS surface fluxes was found to be comparable or even better than results obtained in other studies. The hourly (daily) RMSD for the surface net radiation flux was $54.4 (27.2) \text{ W m}^{-2}$ with correlations of $r=0.96$ ($r = 0.91$) when using tower data as drivers for HOLAPS. For the latent heat flux, the obtained RMSD was $53.0 (35.1) \text{ W m}^{-2}$ with $r = 0.86$ ($r = 0.78$). Using satellite and re-analysis data as only drivers, the RMSD and correlations were found to be 68.9 W m^{-2} and $r = 0.75$ ($42.1, r = 0.63$) for the latent heat flux. Largest uncertainties resulted from the uncertainties of the surface solar radiation flux. However, on monthly timescales, these uncertainties were minimized which indicates that comparable accuracies can be obtained when using satellite based drivers instead of local in-situ data.

A first dataset for HOLAPS is planned to be released to the scientific community after a thorough validation and cross comparison against other datasets like e.g. the LandFlux-Eval (Mueller et al., 2013) data. Further improvements of the HOLAPS framework will comprise the assimilation of land surface temperature data to constrain the

High resolution land surface fluxes from satellite data (HOLAPS v1.0)

A. Loew et al.

Title Page

Abstract

Introduction

Conclusions

References

Tables

Figures



Back

Close

Full Screen / Esc

Printer-friendly Version

Interactive Discussion



surface latent heat flux estimates as well as the usage of new satellite observations like e.g. provided by the new SENTINEL series of satellites.

Appendix A: Acronyms

Acronyms used throughout the text are summarized in Table A1.

5 Appendix B: Detailed HOLAPS model description

The different components of the HOLAPS framework and its land surface model are described in detail in the following sections. The variable definitions used and their units are summarized in Table A1.

B1 HOLAPS runtime environment

10 The general workflow of the HOLAPS runtime environment is illustrated in Fig. B1. After specifying the model setup by the user, the HOLAPS main controller checks the availability of all required data and then launches subprocesses to run the model. Required forcing data is read for each time step and interpolated in space and time if required. Surface water and energy fluxes are calculated for each timestep. Results
15 are then written to netCDF files and additional statistics are calculated if required.

B2 HOLAPS sub-modules

The different sub-modules used within HOLAPS are described in the following.

B2.1 Surface energy balance

The surface energy balance is given as:

$$20 R_N - LE - H - G = 0$$

(B1)

10803

GMDD

8, 10783–10841, 2015

High resolution land surface fluxes from satellite data (HOLAPS v1.0)

A. Loew et al.

Title Page

Abstract

Introduction

Conclusions

References

Tables

Figures

⏪

⏩

◀

▶

Back

Close

Full Screen / Esc

Printer-friendly Version

Interactive Discussion



R_N is estimated from the shortwave and longwave radiation fluxes as:

$$R_N = (1 - \alpha)S^\downarrow + \varepsilon L^\downarrow - \varepsilon\sigma T_s^4 \quad (\text{B2})$$

B2.2 Radiation module

Shortwave solar surface radiation fluxes

5 The shortwave clear sky solar radiation flux ($S_{\text{clear}}^\downarrow$) is estimated using the MAGIC radiative transfer model (Mueller et al., 2009). The shortwave surface downwelling solar flux (S^\downarrow) for all sky conditions is then obtained from the clear-sky downwelling solar flux and the clear sky index k as (Posselt et al., 2012)

$$S^\downarrow = k(\text{CAL})S_{\text{clear}}^\downarrow \quad (\text{B3})$$

10 The clear sky index is related to CAL through the following relationship (Hammer et al., 2003)

$$k = \begin{cases} 1.2 & \text{CAL} \leq -0.2 \\ 1 - \text{CAL} & -0.2 < \text{CAL} \leq 0.8 \\ a + b \cdot \text{CAL} + c \cdot \text{CAL}^2 & 0.8 < \text{CAL} \leq 1.1 \\ 0.05 & \text{CAL} > 1.1 \end{cases} \quad (\text{B4})$$

where $a = 2.0667$, $b = -3.667$, $c = 1.6667$.

Longwave surface radiation fluxes

15 The longwave surface downwelling radiation flux (L^\downarrow) depends on the near surface moisture and temperature profile as well as the cloud coverage. The clear sky longwave downwelling radiation flux $L_{\text{slab}}^\downarrow$ is calculated using the PBL model (Margulis and Entekhabi, 2001). $L_{\text{slab}}^\downarrow$ is then corrected for cloud coverage as (Brubaker and Entekhabi, 1995):

$$20 L_\downarrow = L_{\text{slab}}^\downarrow (1 + 0.17c^2) \quad (\text{B5})$$

B2.3 Soil module

The surface temperature T_s [K] is obtained by a revised force restore approach (Ren and Xue, 2004) as:

$$\frac{\partial T_s}{\partial t} = C_G (R_N - LE - H) - \omega (T_s - T_d - \pi d \gamma_s) - AB'' \sin[\omega t + a''] \quad (\text{B6})$$

5 where A [K] is the diurnal temperature amplitude of T_s , $C_G = 2 \left(\Gamma \sqrt{86\,400\pi} \right)^{-1}$ $\text{K m}^2 \text{J}^{-1}$ is the thermal inertia coefficient and Γ is the thermal inertia which is estimated as function of soil moisture conditions (Murray and Verhoef, 2007).

The parameters B'' and a'' in Eq. (B6) are set to $a'' = 0.45\pi$ and $B'' = 0.158$ (Ren and Xue, 2004). The prognostic equation for the deep soil layer temperature T_d is

$$10 \quad \frac{\partial T_d}{\partial t} = -\frac{1}{\tau} (T_d - T_s + \gamma_s \pi d) \quad (\text{B7})$$

where d is the soil temperature damping scale depth with typical values in the order of $d = 0.15$ m. The lapse rate between the mean surface and deep-layer temperature γ_s K m^{-1} is estimated from the differences between T_s and T_d and $\tau = 86\,400$ s is the time period, one day in our case.

15 B2.4 Water balance module

The surface water balance is defined as

$$P - \frac{\partial I}{\partial t} - Q - ET - \frac{\partial W}{\partial t} = 0 \quad (\text{B8})$$

The soil moisture dynamics is calculated using a multilayer soil scheme, discretized into 5 layers. The soil layers have a thickness of $dz = [0.05, 0.1, 0.25, 0.6, 1.0]$ m. Soil

High resolution land surface fluxes from satellite data (HOLAPS v1.0)

A. Loew et al.

Title Page

Abstract

Introduction

Conclusions

References

Tables

Figures

⏪

⏩

◀

▶

Back

Close

Full Screen / Esc

Printer-friendly Version

Interactive Discussion



moisture fluxes between the different soil layers are simulated by solving numerically the Richards equation (Richards, 1931):

$$\frac{\partial m_v}{\partial t} = \frac{\partial}{\partial z} \left[K(m_v) \left(\frac{\partial \psi}{\partial z} + 1 \right) \right] \quad (\text{B9})$$

The water interception by the canopy is estimated by (Valente et al., 1997)

$$\frac{\partial I}{\partial t} = P - ET_1 - D \quad (\text{B10})$$

where $ET_1 = \lambda^{-1} LE_i$ is the transpiration from the canopy interception storage and D is the through fall and drainage of water from the canopy layer to the soil.

B2.5 Turbulent flux module

For a vegetated patch with fractional vegetation coverage f_c the surface latent heat flux is calculated as the weighted sum of the evaporation from soil (LE_S), the transpiration from the canopy (LE_c) as well as evaporation from water intercepted by the canopy layer (LE_i) as

$$LE = (1 - f_c)LE_S + f_c [(1 - w_I)LE_c + w_I LE_i] \quad (\text{B11})$$

where $w_I = (I/I_{\max})^b$ is a weighting factor dependent on the current canopy interception storage I , the potential maximum interception storage $I_{\max}(\Lambda)$ (von Hoyningen-Huene, 1981) and an empirical parameter $b = 0.5$ (Chen and Dudhia, 2001). The vegetation cover fraction f_c is obtained from leaf area index (Λ) as (Norman et al., 1995):

$$f_c = 1 - e^{-0.5\Lambda} \quad (\text{B12})$$

which assumes a random leaf distribution with spherical leaf angle distribution. The different latent heat flux components in Eq. (14) are then estimated using the Priestley-

Title Page

Abstract

Introduction

Conclusions

References

Tables

Figures

◀

▶

◀

▶

Back

Close

Full Screen / Esc

Printer-friendly Version

Interactive Discussion



Taylor approach as:

$$LE_s = \phi \alpha_p R_{N,S} \frac{\Delta}{\Delta + \gamma} \quad (B13)$$

$$LE_c = \phi \alpha_p R_{N,c} \frac{\Delta}{\Delta + \gamma}$$

$$LE_j = \alpha_p R_{N,c} \frac{\Delta}{\Delta + \gamma}$$

5 where $\alpha_{pt} = 1.26$ is the Priestley-Taylor parameter for equilibrium evapotranspiration and Δ , γ are the slope of the water vapor saturation curve and psychrometer constant (Pa K^{-1}) respectively. The inhibition function $0 \leq [\phi] \leq 1$ describes the reduction of LE due to limiting factors like radiation, temperature and soil moisture. The soil net radiation is estimated as (Norman et al., 1995):

$$10 R_{N,S} = R_N e^{0.9 \ln(1-f_c)} \quad (B14)$$

and the canopy net radiation is then calculated as

$$R_{N,C} = R_N - R_{N,S} \quad (B15)$$

The sensible heat flux is estimated as:

$$H = \rho c_p (T_s - T_a) / r_a \quad (B16)$$

15 where the aerodynamic surface resistance r_a (s m^{-1}) is calculated as:

$$r_a = \left[\left(\log \frac{z-d}{z_{0,m}} - \Psi_m \right) \left(\log \frac{z-d}{z_{0,h}} - \Psi_h \right) \right] [k^2 u_z]^{-1} \quad (B17)$$

where $k \approx 0.41$ is the von Karman constant. The stability correction functions $\Psi_{m,h}$ are calculated after (Paulson, 1970) using the Richardson number Ri as an indicator for atmospheric stability. The roughness lengths for momentum and heat ($z_{0,m}$, $z_{0,h}$) are parameterized for each landcover type (Table B1).

20

High resolution land surface fluxes from satellite data (HOLAPS v1.0)

A. Loew et al.

Title Page	
Abstract	Introduction
Conclusions	References
Tables	Figures
◀	▶
◀	▶
Back	Close
Full Screen / Esc	
Printer-friendly Version	
Interactive Discussion	



Appendix C: Fluxnet stations

Table C1 lists all FLUXNET stations ($N = 49$) that are used in this study.

Appendix D: Ancillary HOLAPS evaluation results

Error statistic for HOLAPS daily and monthly LE and R_N .

5 Code availability

Code for this paper is available from the corresponding author on request. A publication of the HOLAPS code in a public repository is envisaged as part of later releases.

10 *Acknowledgements.* This study was supported through the Cluster of Excellence CliSAP (EXC177), University of Hamburg, funded through the German Science Foundation (DFG) which is gratefully acknowledged. Dissemination of the FLUXNET data through <http://www.fluxdata.org/> and the work of the individual PIs for FLUXNET stations are very much appreciated. EUMETSAT Satellite Application Facility on Climate Monitoring (CM SAF) climate data products were used by permission of Deutscher Wetterdienst. We thank ECMWF for the use of their ERA-Interim re-analysis, NASA for the dissemination and use of the TMPA satellite product, NCDC at NOAA for the dissemination and use of the GridSat radiation
15 satellite product, Beijing Normal University for the provision and use of their enhanced MODIS LAI data and the MODIS land team as well as the ESA Globalbedo project for the provision of land surface parameters.

20 The article processing charges for this open-access publication were covered by the Max Planck Society.

High resolution land surface fluxes from satellite data (HOLAPS v1.0)

A. Loew et al.

Title Page

Abstract

Introduction

Conclusions

References

Tables

Figures



Back

Close

Full Screen / Esc

Printer-friendly Version

Interactive Discussion



References

- Allard, V., Ourcival, J. M., Rambal, S., Joffre, R., and Rocheteau, A.: Seasonal and annual variation of carbon exchange in an evergreen Mediterranean forest in southern France, *Glob. Change Biol.*, 14, 714–725, 2008.
- 5 Ammann, C., Flechard, C. R., Leifeld, J., Neftel, A., and Fuhrer, J.: The carbon budget of newly established temperate grassland depends on management intensity, *Agriculture, Ecosyst. Environ.*, 121, 5–20, 2007.
- Anderson, M. C., Norman, J. M., Mecikalski, J. R., Otkin, J. A., and Kustas, W. P.: A climatological study of evapotranspiration and moisture stress across the continental United States based on thermal remote sensing: 1. Model formulation, *J. Geophys. Res.-Atmos.*, 112, D10117, doi:10.1029/2006JD007506, 2007.
- 10 Aubinet, M., Chermanne, B., Vandenhaute, M., Longdoz, B., Yernaux, M., and Laitat, E.: Long term carbon dioxide exchange above a mixed forest in the Belgian Ardennes, *Agr. Forest Meteorol.*, 108, 293–315, 2001.
- 15 Baldocchi, D.: “Breathing”; of the terrestrial biosphere: lessons learned from a global network of carbon dioxide flux measurement systems, *Austr. J. Botany*, 56, 1–26, 2008.
- Baldocchi, D., Falge, E., Gu, L., Olson, R., Hollinger, D., Running, S., Anthoni, P., Bernhofer, C., Davis, K., Evans, R., Fuentes, J., Goldstein, A., Katul, G., Law, B., Lee, X., Malhi, Y., Meyers, T., Munger, W., Oechel, W., Paw, K. T., Pilegaard, K., Schmid, H. P., Valentini, R., Verma, S., Vesala, T., Wilson, K., and Wofsy, S.: FLUXNET: A New Tool to Study the Temporal and Spatial Variability of Ecosystem–Scale Carbon Dioxide, Water Vapor, and Energy Flux Densities, *B. Am. Meteorol. Soc.*, 82, 2415–2434, 2001.
- 20 Baldocchi, D. D.: Assessing the eddy covariance technique for evaluating carbon dioxide exchange rates of ecosystems: past, present and future, *Glob. Change Biol.*, 9, 479–492, 2003.
- 25 Baldocchi, D. D., Xu, L., and Kiang, N.: How plant functional-type, weather, seasonal drought, and soil physical properties alter water and energy fluxes of an oak–grass savanna and an annual grassland, *Agr. Forest Meteorol.*, 123, 13–39, 2004.
- Beljaars, A. and Bosveld, F.: Cabauw data for the validation of land surface parameterization schemes, *J. Climate*, 1997, 1172–1193, 1997.
- 30 Berbigier, P., Bonnefond, J.-M., and Mellmann, P.: CO₂ and water vapour fluxes for 2 years above Euroflux forest site, *Agr. Forest Meteorol.*, 108, 183–197, 2001.

High resolution land surface fluxes from satellite data (HOLAPS v1.0)

A. Loew et al.

Title Page

Abstract

Introduction

Conclusions

References

Tables

Figures



Back

Close

Full Screen / Esc

Printer-friendly Version

Interactive Discussion



High resolution land surface fluxes from satellite data (HOLAPS v1.0)

A. Loew et al.

[Title Page](#)

[Abstract](#)

[Introduction](#)

[Conclusions](#)

[References](#)

[Tables](#)

[Figures](#)

[⏪](#)

[⏩](#)

[◀](#)

[▶](#)

[Back](#)

[Close](#)

[Full Screen / Esc](#)

[Printer-friendly Version](#)

[Interactive Discussion](#)



Bontemps, S., Defourny, P., Brockmann, C., Herold, M., Kalogirou, V., and Arino, O.: New global land cover mapping exercise in the framework of the ESA Climate Change Initiative, 44–47, 2012.

Brubaker, K. L. and Entekhabi, D.: An analytic approach to modeling land-atmosphere interaction: 1. Construct and equilibrium behavior, *Water Resour. Res.*, 31, 619–632, 1995.

Chen, B., Coops, N. C., Fu, D., Margolis, H. a., Amiro, B. D., Barr, A. G., Black, T. A., Arain, M. A., Bourque, C. P.-A., Flanagan, L. B., Lafleur, P. M., McCaughey, J. H., and Wofsy, S. C.: Assessing eddy-covariance flux tower location bias across the Fluxnet-Canada Research Network based on remote sensing and footprint modelling, *Agr. Forest Meteorol.*, 151, 87–100, 2011.

Chen, F. and Dudhia, J.: Coupling an Advanced Land Surface–Hydrology Model with the Penn State–NCAR MM5 Modeling System. Part I: Model Implementation and Sensitivity, *Mon. Weather Rev.*, 129, 569–585, 2001.

Chiesi, M., Maselli, F., Bindi, M., Fibbi, L., Cherubini, P., Arlotta, E., Tirone, G., Matteucci, G., and Seufert, G.: Modelling carbon budget of Mediterranean forests using ground and remote sensing measurements, *Agr. Forest Meteorol.*, 135, 22–34, 2005.

Clark, K. L., Gholz, H. L., and Castro, M. S.: Carbon dynamics along a chronosequence of slash pine plantations in north Florida, *Ecol. Appl.*, 14, 1154–1171, 2004.

Cook, B. D., Davis, K. J., Wang, W., Desai, A., Berger, B. W., Teclaw, R. M., Martin, J. G., Bolstad, P. V., Bakwin, P. S., Yi, C., and Heilman, W.: Carbon exchange and venting anomalies in an upland deciduous forest in northern Wisconsin, USA, *Agr. Forest Meteorol.*, 126, 271–295, 2004.

Cosby, B., Hornberger, G., Clapp, R., and Ginn, T.: A statistical exploration of the relationships of soil moisture characteristics to the physical properties of soils, *Water Resour. Res.*, 20, 682–690, 1984.

Dee, D. P., Uppala, S. M., Simmons, A. J., Berrisford, P., Poli, P., Kobayashi, S., Andrae, U., Balmaseda, M. A., Balsamo, G., Bauer, P., Bechtold, P., Beljaars, A. C. M., van de Berg, L., Bidlot, J., Bormann, N., Delsol, C., Dragani, R., Fuentes, M., Geer, A. J., Haimberger, L., Healy, S. B., Hersbach, H., Hólm, E. V., Isaksen, L., Kållberg, P., Köhler, M., Matricardi, M., McNally, A. P., Monge-Sanz, B. M., Morcrette, J. J., Park, B. K., Peubey, C., de Rosnay, P., Tavolato, C., Thépaut, J. N., and Vitart, F.: The ERA-Interim reanalysis: configuration and performance of the data assimilation system, *Q. J. R. Meteor. Soc.*, 137, 553–597, 2011.

High resolution land surface fluxes from satellite data (HOLAPS v1.0)

A. Loew et al.

Title Page

Abstract

Introduction

Conclusions

References

Tables

Figures



Back

Close

Full Screen / Esc

Printer-friendly Version

Interactive Discussion



- Gond, V., De Pury, D. G. G., Veroustraete, F., and Ceulemans, R.: Seasonal variations in leaf area index, leaf chlorophyll, and water content; scaling-up to estimate fAPAR and carbon balance in a multilayer, multispecies temperate forest, *Tree Physiol.*, 19, 673–679, 1999.
- Gouldon, M. L., Winston, G. C., McMillan, A. M. S., Litvak, M. E., Read, E. L., Rocha, A. V., and Rob Elliot, J.: An eddy covariance mesonet to measure the effect of forest age on land-atmosphere exchange, *Glob. Change Biol.*, 12, 2146–2162, 2006.
- Granier, a., Ceschia, E., Damesin, C., Dufrene, E., Epron, D., Gross, P., Lebaube, S., Le Dantec, V., Le Goff, N., Lemoine, D., Lucot, E., Ottorini, J. M., Pontailler, J. Y., and Saugier, B.: The carbon balance of a young Beech forest, *Func. Ecol.*, 14, 312–325, 2000.
- Gu, L., Meyers, T., Pallardy, S. G., Hanson, P. J., Yang, B., Heuer, M., Hosman, K. P., Liu, Q., Riggs, J. S., Sluss, D., and Wullschleger, S. D.: Influences of biomass heat and biochemical energy storages on the land surface fluxes and radiative temperature, *J. Geophys. Res.*, 112, 1–11, 2007.
- Gu, L., Meyers, T., Pallardy, S. G., Hanson, P. J., Yang, B., Heuer, M., Hosman, K. P., Riggs, J. S., Sluss, D., and Wullschleger, S. D.: Direct and indirect effects of atmospheric conditions and soil moisture on surface energy partitioning revealed by a prolonged drought at a temperate forest site, *J. Geophys. Res.*, 111, 1–13, 2006.
- Hagemann, S.: An improved land surface parameter dataset for global and regional climate models Max-Planck-Institute for Meteorology, 2002.
- Hammer, A., Heinemann, D., Hoyer, C., Kuhlemann, R., Lorenz, E., Müller, R., and Beyer, H. G.: Solar energy assessment using remote sensing technologies, *Remote Sens. Environ.*, 86, 423–432, 2003.
- Hollinger, D. Y., Aber, J., Dail, B., Davidson, E. a., Goltz, S. M., Hughes, H., Leclerc, M. Y., Lee, J. T., Richardson, A. D., Rodrigues, C., Scott, N. a., Achuatavarier, D., and Walsh, J.: Spatial and temporal variability in forest-atmosphere CO₂ exchange, *Glob. Change Biol.*, 10, 1689–1706, 2004.
- Huffman, G. J., Bolvin, D. T., Nelkin, E. J., Wolff, D. B., Adler, R. F., Gu, G., Hong, Y., Bowman, K. P., and Stocker, E. F.: The TRMM Multisatellite Precipitation Analysis (TMPA): Quasi-Global, Multiyear, Combined-Sensor Precipitation Estimates at Fine Scales, *J. Hydrometeorol.*, 8, 38–55, 2007.
- Hutley, L. B., O’Grady, A. P., and Eamus, D.: Evapotranspiration from Eucalypt open-forest savanna of Northern Australia, *Funct. Ecol.*, 14, 183–194, 2000.

High resolution land surface fluxes from satellite data (HOLAPS v1.0)

A. Loew et al.

[Title Page](#)
[Abstract](#)
[Introduction](#)
[Conclusions](#)
[References](#)
[Tables](#)
[Figures](#)
[Back](#)
[Close](#)
[Full Screen / Esc](#)
[Printer-friendly Version](#)
[Interactive Discussion](#)


Ingwersen, J., Imukova, K., Högy, P., and Streck, T.: On the use of the post-closure methods uncertainty band to evaluate the performance of land surface models against eddy covariance flux data, *Biogeosciences*, 12, 2311–2326, doi:10.5194/bg-12-2311-2015, 2015.

Jiménez, C., Prigent, C., Mueller, B., Seneviratne, S. I., McCabe, M. F., Wood, E. F., Rossow, W. B., Balsamo, G., Betts, a. K., Dirmeyer, P. a., Fisher, J. B., Jung, M., Kanamitsu, M., Reichle, R. H., Reichstein, M., Rodell, M., Sheffield, J., Tu, K., and Wang, K.: Global intercomparison of 12 land surface heat flux estimates, *J. Geophys. Res.*, 116, 1–27, 2011.

Jung, M., Reichstein, M., Margolis, H. A., Cescatti, A., Richardson, A. D., Arain, M. A., Arneeth, A., Bernhofer, C., Bonal, D., Chen, J., Gianelle, D., Gobron, N., Kiely, G., Kutsch, W., Lasslop, G., Law, B. E., Lindroth, A., Merbold, L., Montagnani, L., Moors, E. J., Papale, D., Sottocornola, M., Vaccari, F., and Williams, C.: Global patterns of land-atmosphere fluxes of carbon dioxide, latent heat, and sensible heat derived from eddy covariance, satellite, and meteorological observations, *J. Geophys. Res.*, 116, G00J07, doi:10.1029/2010JG001566, 2011.

Justice, C., Townshend, J., Vermote, E., Masuoka, E., Wolfe, R. E., Saleous, N., Roy, D. P., and Morisette, J. T.: An overview of MODIS Land data processing and product status, *Remote Sens. Environ.*, 83, 3–15, 2002.

Kalma, J., McVicar, T., and McCabe, M.: Estimating Land Surface Evaporation: A Review of Methods Using Remotely Sensed Surface Temperature Data, *Surv. Geophys.*, 29, 421–469, 2008.

Kidd, C., Bauer, P., Turk, J., Huffman, G. J., Joyce, R., Hsu, K.-L., and Braithwaite, D.: Intercomparison of High-Resolution Precipitation Products over Northwest Europe, *J. Hydrometeorol.*, 13, 67–83, 2012.

Kim, C. P. and Entekhabi, D.: Feedbacks in the Land-Surface and Mixed-Layer Energy Budgets, *Bound.-Lay. Meteorol.*, 88, 1–21, 1998.

Kinne, S., O'Donnel, D., Stier, P., Kloster, S., Zhang, K., Schmidt, H., Rast, S., Giorgetta, M., Eck, T. F., and Stevens, B.: MAC-v1: A new global aerosol climatology for climate studies, *J. Adv. Model. Earth Syst.*, 5, 704–740, 2013.

Knapp, K. R.: Scientific data stewardship of international satellite cloud climatology project B1 global geostationary observations, *J. Appl. Remote Sens.*, 2, 023548, doi:10.1117/1.3043461, 2008.

Knapp, K. R., Ansari, S., Bain, C. L., Bourassa, M. A., Dickinson, M. J., Funk, C., Helms, C. N., Hennon, C. C., Holmes, C. D., Huffman, G. J., Kossin, J. P., Lee, H.-T., Loew, A.,

High resolution land surface fluxes from satellite data (HOLAPS v1.0)

A. Loew et al.

Title Page

Abstract

Introduction

Conclusions

References

Tables

Figures

◀

▶

◀

▶

Back

Close

Full Screen / Esc

Printer-friendly Version

Interactive Discussion



- Myneni, R. B., Hoffman, S., Knyazikhin, Y., Privette, J. L., Glassy, J., Tian, Y., Wang, Y., Song, X., Zhang, Y., Smith, G. R., Lotsch, A., Friedl, M., Morisette, J. T., Votava, P., Nemani, R. R., and Running, S. W.: Global products of vegetation leaf area and fraction absorbed PAR from year one of MODIS data, *Remote Sens. Environ.*, 83, 214–231, 2002.
- 5 Nagy, Z., Pintér, K., Czóbel, S., Balogh, J., Horváth, L., Fóti, S., Barcza, Z., Weidinger, T., Csintalan, Z., Dinh, N. Q., Grosz, B., and Tuba, Z.: The carbon budget of semi-arid grassland in a wet and a dry year in Hungary, *Agr. Ecosyst. Environ.*, 121, 21–29, 2007.
- Norman, J. M., Kustas, W. P., and Humes, K. S.: Source approach for estimating soil and vegetation energy fluxes in observations of directional radiometric surface temperature, *Agr. Forest Meteorol.*, 77, 263–293, 1995.
- 10 Papale, D., Agarwal, D., Baldocchi, D., Cook, R., Fisher, J., and van Ingen, C.: Database Maintenance, Data Sharing Policy, Collaboration, in: *Eddy Covariance*, edited by: Aubinet, M., Vesala, T., and Papale, D., Springer Atmospheric Sciences, Springer Netherlands, 2012.
- Paulson, C. A.: The Mathematical Representation of Wind Speed and Temperature Profiles in the Unstable Atmospheric Surface Layer, *J. Appl. Meteorol.*, 9, 857–861, 1970.
- 15 Peng, J., Liu, Y., Zhao, X., and Loew, A.: Estimation of evapotranspiration from MODIS TOA radiances in the Poyang Lake basin, China, *Hydrol. Earth Syst. Sci.*, 17, 1431–1444, 2013, <http://www.hydrol-earth-syst-sci.net/17/1431/2013/>.
- Peng, J. and Loew, A.: Evaluation of Daytime Evaporative Fraction from MODIS TOA Radiances Using FLUXNET Observations, *Remote Sens.*, 6, 5959, doi:10.3390/rs6075959, 2014.
- 20 Posselt, R., Mueller, R. W., Stöckli, R., and Trentmann, J.: Remote sensing of solar surface radiation for climate monitoring – the CM-SAF retrieval in international comparison, *Remote Sens. Environ.*, 118, 186–198, 2012.
- Potts, D. R., Mackin, S., Muller, J. P., and Fox, N.: Sensor Intercalibration Over Dome C for the ESA GlobAlbedo Project, *Geosci. Remote Sens.*, 51, 1139–1146, 2013.
- 25 Rawls, W. J. and Brakensiek, D.: Prediction of soil water properties for hydrologic modeling, 293–299, 1985.
- Rebmann, C., Zeri, M., Lasslop, G., Mund, M., Kolle, O., Schulze, E.-D., and Feigenwinter, C.: Treatment and assessment of the CO₂-exchange at a complex forest site in Thuringia, Germany, *Agr. Forest Meteorol.*, 150, 684–691, 2010.
- 30 Ren, D. and Xue, M.: A Revised Force–Restore Model for Land Surface Modeling, *J. Appl. Meteorol.*, 43, 1768–1782, 2004.

High resolution land surface fluxes from satellite data (HOLAPS v1.0)

A. Loew et al.

Title Page

Abstract

Introduction

Conclusions

References

Tables

Figures



Back

Close

Full Screen / Esc

Printer-friendly Version

Interactive Discussion



- Richards, L. A.: Capillary conduction of liquids through porous mediums, *J. Appl. Phys.*, 1, 318–333, 1931.
- Roads, J. and Betts, A.: NCEP–NCAR and ECMWF Reanalysis Surface Water and Energy Budgets for the Mississippi River Basin, *J. Hydrometeorol.*, 1, 88–94, 2000.
- 5 Roerink, G. J., Su, Z., and Menenti, M.: S-SEBI: A simple remote sensing algorithm to estimate the surface energy balance, *Phys. Chem. Earth Pt. B*, 25, 147–157, 2000.
- Rossow, W. W. B. and Schiffer, R. A. R.: ISCCP Cloud Data Products, *B. Am. Meteorol. Soc.*, 72, 2–20, 1991.
- Scherer-Lorenzen, M., Schulze, E., Don, A., Schumacher, J., and Weller, E.: Exploring the functional significance of forest diversity: A new long-term experiment with temperate tree species (BIOTREE), *Perspect. Plant Ecol.*, 9, 53–70, 2007.
- 10 Smeda, M.: A bulk model for the atmospheric planetary boundary layer, *Bound.-Lay. Meteorol.*, 17, 411–427, 1979.
- Su, Z.: The Surface Energy Balance System (SEBS) for estimation of turbulent heat fluxes, *Hydrol. Earth Syst. Sci.*, 6, 85–100, doi:10.5194/hess-6-85-2002, 2002.
- Tang, R., Li, Z.-L., and Chen, K.-S.: Validating MODIS-derived land surface evapotranspiration with in situ measurements at two AmeriFlux sites in a semiarid region, *J. Geophys. Res.*, 116, D04106, doi:10.1029/2010JD014543, 2011.
- Taylor, K. E.: Summarizing multiple aspects of model performance in a single diagram, *J. Geophys. Res.*, 106, 7183–7192, 2001.
- 20 Tedeschi, V., Rey, A., Manca, G., Valentini, R., Jarvis, P. G., and Borghetti, M.: Soil respiration in a Mediterranean oak forest at different developmental stages after coppicing, *Glob. Change Biol.*, 12, 110–121, 2006.
- Twine, T. E., Kustas, W. P., Norman, J. M., Cook, D. R., Houser, P. R., Meyers, T. P., Prueger, J. H., Starks, P. J., and Wesely, M. L.: Correcting eddy-covariance flux underestimates over a grassland, *Agr. Forest Meteorol.*, 103, 279–300, 2000.
- 25 Valente, F., David, J. S., and Gash, J. H. C.: Modelling interception loss for two sparse eucalypt and pine forests in central Portugal using reformulated Rutter and Gash analytical models, *J. Hydrol.*, 190, 141–162, 1997.
- 30 Verma, S. B., Dobermann, A., Cassman, K. G., Walters, D. T., Knops, J. M., Arkebauer, T. J., Suyker, A. E., Burba, G. G., Amos, B., Yang, H., Ginting, D., Hubbard, K. G., Gitelson, A. A., and Walter-Shea, E. A.: Annual carbon dioxide exchange in irrigated and rainfed maize-based agroecosystems, *Agr. Forest Meteorol.*, 131, 77–96, 2005.

High resolution land surface fluxes from satellite data (HOLAPS v1.0)

A. Loew et al.

Title Page

Abstract

Introduction

Conclusions

References

Tables

Figures

◀

▶

◀

▶

Back

Close

Full Screen / Esc

Printer-friendly Version

Interactive Discussion



- Vinukollu, R. K., Wood, E. F., Ferguson, C. R., and Fisher, J. B.: Global estimates of evapotranspiration for climate studies using multi-sensor remote sensing data: Evaluation of three process-based approaches, *Remote Sens. Environ.*, 115, 801–823, 2011.
- von Hoyningen-Huene, J.: Die Interzeption des Niederschlags in landwirtschaftlichen Pflanzenbeständen, *Arbeitsbericht Deutscher Verband für Wasserwirtschaft und Kulturbau, DVWK*, 1981.
- Wang, K. and Dickinson, R. E.: A review of global terrestrial evapotranspiration: Observation, modeling, climatology, and climatic variability, *Rev. Geophys.*, 50, RG2005, doi:10.1029/2011RG000373, 2012.
- Wilson, K., Goldstein, A., Falge, E., Aubinet, M., Baldocchi, D., Berbigier, P., Bernhofer, C., Ceulemans, R., Dolman, H., Field, C., Grelle, A., Ibrom, A., Law, B. E., Kowalski, A., Meyers, T., Moncrieff, J., Monson, R., Oechel, W., Tenhunen, J., Valentini, R., and Verma, S.: Energy balance closure at FLUXNET sites, *Agr. Forest Meteorol.*, 113, 223–243, 2002.
- Wohlfahrt, G., Hammerle, A., Haslwanter, A., Bahn, M., Tappeiner, U., and Cernusca, A.: Seasonal and inter-annual variability of the net ecosystem CO₂ exchange of a temperate mountain grassland: Effects of weather and management, *J. Geophys. Res.*, 113, D08110, doi:10.1029/2007JD009286, 2008.
- Wösten, J. H. M., Pachepsky, Y. A., and Rawls, W. J.: Pedotransfer functions: bridging the gap between available basic soil data and missing soil hydraulic characteristics, *J. Hydrol.*, 251, 123–150, 2001.
- Yang, F., Zhu, A.-X., Ichii, K., White, M. A., Hashimoto, H., and Nemani, R. R.: Assessing the representativeness of the AmeriFlux network using MODIS and GOES data, *J. Geophys. Res.*, 113, G04036, doi:10.1029/2007JG000627, 2008.
- Yuan, H., Dai, Y., Xiao, Z., Ji, D., and Shangguan, W.: Reprocessing the MODIS Leaf Area Index products for land surface and climate modelling, *Remote Sens. Environ.*, 115, 1171–1187, 2011.
- Zhang, X., Berhane, T., and Seielstad, G.: Comparison of Landsat and MODIS Estimates of Heat Fluxes: Effect of Surface Heterogeneity, 759–762, 2008.

High resolution land surface fluxes from satellite data (HOLAPS v1.0)

A. Loew et al.

Title Page

Abstract

Introduction

Conclusions

References

Tables

Figures

⏪

⏩

◀

▶

Back

Close

Full Screen / Esc

Printer-friendly Version

Interactive Discussion



Table 2. List of performed model experiments. Includes the number of stations and station years as well as the data source: *F* = FLUXNET data; *S* = satellite data for precipitation and radiation; additional data from satellite for albedo and LAI, and from ECMWF reanalyses for temperature, total column water vapor, and wind speed.

Coverage	Experiment	Number of		Precipitation		Radiation		Temperature		Wind speed	
		stations	years	<i>F</i>	<i>S</i>	<i>F</i>	<i>S</i>	<i>F</i>	<i>S</i>	<i>F</i>	<i>S</i>
Global	CTRL_G	49	103	x		x		x		x	
Metosat disk	CTRL_M	19	37	x		x		x		x	
	METEOSAT_M	19	37	x			x	x		x	
	GRIDSAT_M	19	37	x			x	x		x	
Global	GRIDSAT_G	49	103	x			x	x		x	
±50°	CTRL_50	31	63	x		x		x		x	
	GRIDSAT_50	31	63	x			x	x		x	
	Tmpa_50	31	63		x	x		x		x	
	Ta_50	31	63	x		x			x	x	
	Wind_50	31	63	x		x		x			x
Metosat disk & ±50°	CTRL_M_50	10	17	x		x		x		x	
	METEOSAT_M_50	10	17		x		x		x		x
	GRIDSAT_M_50	10	17		x		x		x		x

High resolution land surface fluxes from satellite data (HOLAPS v1.0)

A. Loew et al.

Title Page

Abstract

Introduction

Conclusions

References

Tables

Figures

⏪

⏩

◀

▶

Back

Close

Full Screen / Esc

Printer-friendly Version

Interactive Discussion



Table 3. Overall HOLAPS accuracies for R_N , LE and S^l at hourly (h), daily (d) and monthly (m) timescales for the CTRL, GRIDSAT and METEOSAT experiments.

Variable	Experiment	RMSD (W m^{-2})			cRMSD (W m^{-2})			R		
		H	D	M	H	D	M	H	D	M
R_N	CTRL_G	54.4	27.2	23.0	54.3	26.9	22.6	0.96	0.91	0.91
	GRIDSAT_G	111.8	50.5	29.5	110.6	47.6	23.6	0.86	0.68	0.90
LE	CTRL_G	53.0	35.1	30.2	51.3	32.1	26.4	0.86	0.78	0.78
	GRIDSAT_G	68.9	42.1	30.1	68.3	40.8	28.1	0.75	0.63	0.75
R_G	METEOSAT_M	142.0	71.7	15.5	141.8	71.2	12.9	0.83	0.73	0.99
	GRIDSAT_M	134.3	70.2	32.3	131.6	64.8	16.6	0.86	0.74	0.98

High resolution land surface fluxes from satellite data (HOLAPS v1.0)

A. Loew et al.

Table A1. Acronyms used throughout the text.

symbol	variable	unit
General variables		
c_p	Heat capacity of dry air	$[\text{J kg}^{-1} \text{K}^{-1}]$
ρ	Density of dry air	$[\text{kg m}^{-3}]$
Δ	Slope of water vapor saturation curve	$[\text{Pa K}^{-1}]$
γ	Psychrometer constant	$[\text{Pa K}^{-1}]$
$\alpha_{\text{pt}} = 1.26$	Priestley Taylor parameter	$[-]$
Λ	Leaf area index	$[\text{m}^2 \text{m}^{-2}]$
ε	surface emissivity	$[-]$
$\sigma = 5.670373 \times 10^{-8}$	Stefan-Boltzmann constant	$[\text{W m}^{-2} \text{K}^{-1}]$
t	Time	$[\text{s}]$
$g = 9.80665$	Gravity acceleration	$[\text{m s}^{-2}]$
T_a	Air temperature (2 m)	$[\text{K}]$
P	Precipitation rate	$[\text{m s}^{-1}]$
Q	Runoff (fast, slow, percolation)	$[\text{m s}^{-1}]$
ET	Evapotranspiration flux	$[\text{m s}^{-1}]$
λ	Latent heat vaporization	$[\text{J kg}^{-1}]$
Radiation module		
CAL	Effective cloud albedo $[0, \dots, 1]$	$[-]$
a	Surface albedo	$[-]$
c	Cloud cover fraction $[0, \dots, 1]$	$[-]$
$R_N, R_{N,S}, R_{N,C}$	Surface net radiation, soil/canopy net radiation	W m^{-2}
$S_{\text{clear}}^{\downarrow}$	Shortwave downwelling flux, clear-sky downwelling flux	W m^{-2}
$L_{\text{slab}}^{\downarrow}$	Longwave downwelling flux, clear-sky longwave downwelling flux	W m^{-2}
k	Clear sky index $[0 \dots 1]$	$[-]$
TCW	Total column water vapor content	kg m^{-2}
PBL module		
H_v	Virtual heat flux	W m^{-2}
H_{top}	Entrainment flux	W m^{-2}
∂_{θ_m}	Mixed layer inversion strength	$[\text{K}]$
θ_m	Boundary layer potential temperature	$[\text{K}]$
k	von Karman constant (≈ 0.41)	$[-]$
$\zeta = 0.01$	Dissipation parameter	$[-]$

Title Page

Abstract

Introduction

Conclusions

References

Tables

Figures

◀

▶

◀

▶

Back

Close

Full Screen / Esc

Printer-friendly Version

Interactive Discussion



Table A1. Continued.

symbol	variable	unit
Turbulent flux module		
u	Wind speed	$[\text{m s}^{-1}]$
LE, LE_i, LE_s, LE_c	Latent heat flux, subscripts indicate: interception, soil, canopy	W m^{-2}
ET	Evapotranspiration	$[\text{m s}^{-1}]$
ET_i	Evapotranspiration from canopy interception storage	$[\text{m s}^{-1}]$
h	Vegetation height	$[\text{m}]$
H	Sensible heat flux	W m^{-2}
G	Soil heat flux	W m^{-2}
u_*	Friction velocity	$[\text{m s}^{-1}]$
f_c	Vegetation cover fraction	$[-]$
r_a	Aerodynamic surface resistance	$[\text{s m}^{-1}]$
$\Psi_{m,h}$	Stability correction functions	
R_i	Richardson number	$[-]$
$z_{0,m}, z_{0,h}$	Roughness lengths for momentum and heat	$[\text{m}]$
ϕ	Vegetation inhibition function	$[-]$
R_r	Aerodynamic resistance	$[\text{s m}^{-1}]$
R_c	Canopy resistance	$[\text{s m}^{-1}]$
r_{rad}	Radiation stress factor	$[\text{W m}^{-2}]$
$r_{\text{min}}, r_{\text{max}}$	minimum and maximum canopy resistance	$[\text{s m}^{-1}]$
$Y_{\theta m}$	Potential temperature lapse rate	$[\text{K m}^{-1}]$
z_{veg}	Vegetation height	$[\text{m}]$
Water flux and soil module		
I, I_{max}	Canopy interception storage, maximum interception storage	$[\text{m}]$
C_G	Thermal inertial coefficient	$[\text{K m}^2 \text{J}^{-1}]$
Γ	Thermal inertia	$[\text{J m}^{-2} \text{K}^{-1} \text{s}^{-0.5}]$
$d = 1.5 \text{ m}$	Soil temperature damping scale depth	$[\text{m}]$
γ_s	Soil temperature lapse rate	$[\text{K m}^{-1}]$
D	Throughfall and drainage of water from the canopy layer to the soil	$[\text{m s}^{-1}]$
T_s	Surface temperature	$[\text{K}]$
T_d	Deep soil temperature	$[\text{K}]$
z	Vertical coordinate (e.g. boundary layer height, soil depth)	$[\text{m}]$
m_v	Volumetric soil moisture	$[\text{m}^3 \text{m}^{-3}]$
Θ	Relative degree of saturation for soil moisture	$[-]$
K	Unsaturated soil conductivity	$[\text{m s}^{-1}]$
Ψ	Soil suction pressure head	$[\text{m}]$
W	Water storage in soil	$[\text{m}]$

High resolution land surface fluxes from satellite data (HOLAPS v1.0)

A. Loew et al.

Title Page

Abstract

Introduction

Conclusions

References

Tables

Figures



Back

Close

Full Screen / Esc

Printer-friendly Version

Interactive Discussion



High resolution land surface fluxes from satellite data (HOLAPS v1.0)

A. Loew et al.

Title Page

Abstract

Introduction

Conclusions

References

Tables

Figures

⏪

⏩

◀

▶

Back

Close

Full Screen / Esc

Printer-friendly Version

Interactive Discussion



Table B1. Land cover specific parameters.

Landcover	α_{pt}	r_{min}	r_{max}	r_{rad}	$z_{0,m}$	$z_{0,h}$	z_{veg}
Bare soil	1.26	400	5000	–	0.001	0.001	–
Cropland	1.26	40	5000	30	0.01	0.001	0.2
Deciduous broadleaf forest	0.91	100	5000	30	1.0	0.1	15
Coniferous forest	0.91	150	5000	30	1.4	0.14	15
Coniferous forest or deciduous	0.91	150	5000	30	1.2	0.14	15
Deciduous broadleaf forest and broad leaf/mixed forest	0.91	100	5000	30	1.0	0.1	15
Grassland	1.26	40	5000	100	0.01	0.001	0.2
Savanna	1.26	300	5000	100	0.01	0.001	0.4
Deciduous broadleaf forest and broad leaf/mixed forest	0.91	100	5000	30	1.0	0.1	15

High resolution land surface fluxes from satellite data (HOLAPS v1.0)

A. Loew et al.

Table C1. List of FLUXNET stations investigated.

N	Station ID	Lat	Lon	Years			Coverage		Reference
				2003	2004	2005	Global	±50° Meteosat	
1	ATNeu	47.12	11.32	X	X		X	X	Wohlfahrt et al. (2008)
2	AUHow	-12.49	131.15	X	X	X	X	X	Hutley et al. (2000)
3	AUTum	-35.66	148.15	X	X	X	X	X	Leuning et al. (2005)
4	BEBra	51.31	4.52		X	X	X		Gond et al. (1999)
5	BEVie	50.31	6.00			X	X	X	Aubinet et al. (2001)
6	CAMan	55.88	-98.48	X			X		Dunn et al. (2007)
7	CAMer	45.41	-75.52	X	X		X	X	Laflaur (2003)
8	CANS1	55.88	-98.48	X	X		X		Gouldon et al. (2006)
9	CANS2	55.91	-98.52	X	X	X	X		Gouldon et al. (2006)
10	CANS3	55.91	-98.38		X	X	X		Gouldon et al. (2006)
11	CANS4	55.91	-98.38	X			X		Gouldon et al. (2006)
12	CANS5	55.86	-98.49	X	X	X	X		Gouldon et al. (2006)
13	CANS6	55.92	-98.96	X	X	X	X		Gouldon et al. (2006)
14	CANS7	56.64	-99.95	X	X	X	X		Gouldon et al. (2006)
15	CAQcu	49.27	-74.04	X	X	X	X	X	
16	CASF3	54.09	-106.01	X	X	X	X		Mkhabela et al. (2009)
17	CHOe1	47.29	7.73	X			X	X	Ammann et al. (2007)
18	CZBK1	49.50	18.54			X	X	X	
19	DEGri	50.95	13.51			X	X	X	Gilmanov et al. (2007)
20	DEHai	51.08	10.45	X	X	X	X	X	Knohl et al. (2003)
21	DEMeh	51.28	10.66		X	X	X	X	Scherer-Lorenzen et al. (2007)
22	DETha	50.96	13.57	X	X	X	X	X	
23	DEWet	50.45	11.46	X	X	X	X	X	Rebmann et al. (2010)
24	FRHes	48.67	7.06	X	X	X	X	X	Granier et al. (2000)
25	FRLBr	44.72	-0.77	X			X	X	Berbigier et al. (2001)
26	FRPue	43.74	3.60		X	X	X	X	Allard et al. (2008)
27	HUBug	46.69	19.60	X	X	X	X	X	Nagy et al. (2007)
28	ITCpz	41.71	12.38		X	X	X	X	Garbulsky et al. (2008)
29	ITRo2	42.39	11.92		X		X	X	Tedeschi et al. (2006)
30	ITSRo	43.73	10.28	X			X	X	Chiesi et al. (2005)
31	NLCA1	51.97	4.93	X	X	X	X	X	Beljaars and Bosveld (1997)
32	NLLoo	52.17	5.74	X	X		X	X	Dolman et al. (2002)
33	USARM	36.61	-97.49	X	X	X	X	X	Fischer et al. (2007)
34	USAud	31.59	-110.51		X	X	X	X	Tang et al. (2011, 2008)
35	USBkg	44.35	-96.84		X	X	X	X	Zhang et al. (2008)
36	USBo1	40.01	-88.29	X	X	X	X	X	Meyers (2004)
37	USFPe	48.31	-105.10	X		X	X	X	Gilmanov et al. (2005), Zhang et al. (2008)
38	USGoo	34.25	-89.87		X		X	X	
39	USHo1	45.20	-68.74	X	X		X	X	Hollinger et al. (2004)
40	USHo2	45.21	-68.75	X	X		X	X	Hollinger et al. (2004)
41	USLos	46.08	-89.98	X	X	X	X	X	
42	USMOz	38.74	-92.20		X	X	X	X	Gu et al. (2007, 2006)
43	USNe1	41.17	-96.48	X	X		X	X	Verma et al. (2005)
44	USNe2	41.16	-96.47	X	X		X	X	Verma et al. (2005)
45	USNe3	41.18	-96.44	X	X		X	X	Verma et al. (2005)
46	USOho	41.55	-83.84		X	X	X	X	
47	USSP2	29.76	-82.24	X	X		X	X	Clark et al. (2004)
48	USTon	38.43	-120.97	X		X	X	X	Baldocchi et al. (2004)
49	USWCr	45.81	-90.08	X		X	X	X	Cook et al. (2004)

Title Page

Abstract Introduction

Conclusions References

Tables Figures

◀ ▶

◀ ▶

Back Close

Full Screen / Esc

Printer-friendly Version

Interactive Discussion



GMDD

8, 10783–10841, 2015

High resolution land surface fluxes from satellite data (HOLAPS v1.0)

A. Loew et al.

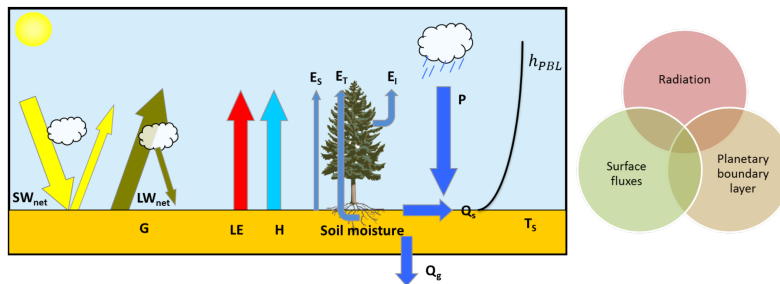


Figure 2. HOLAPS estimated fluxes and modules.

Title Page

Abstract

Introduction

Conclusions

References

Tables

Figures

◀

▶

◀

▶

Back

Close

Full Screen / Esc

Printer-friendly Version

Interactive Discussion



High resolution land surface fluxes from satellite data (HOLAPS v1.0)

A. Loew et al.

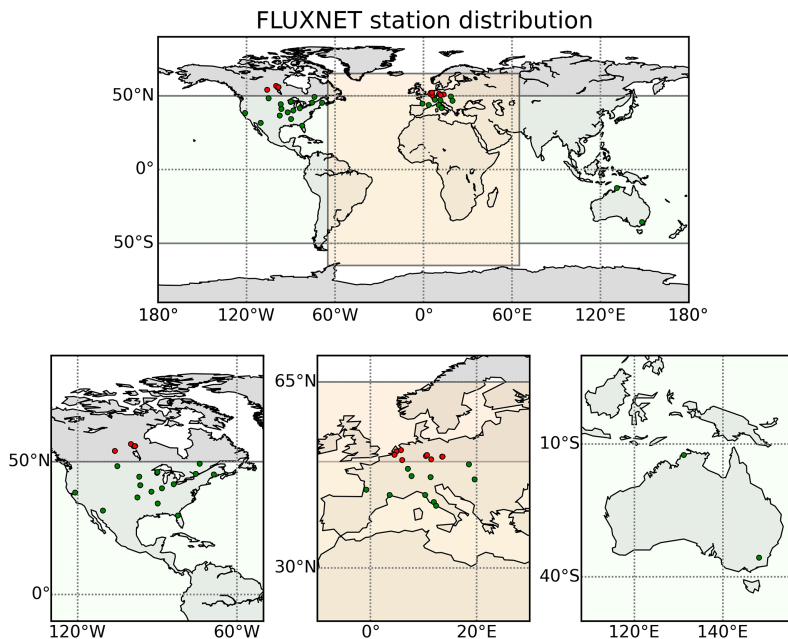


Figure 3. Distribution of FLUXNET stations used in this study. Light green corresponds to latitudes between 50° N and 50° S which corresponds to the coverage of the TMPA precipitation data (see text). Stations in red cannot be used when forced with TMPA data. Light orange indicates approximate coverage of Meteosat data.

[Title Page](#)
[Abstract](#)
[Introduction](#)
[Conclusions](#)
[References](#)
[Tables](#)
[Figures](#)
[⏪](#)
[⏩](#)
[◀](#)
[▶](#)
[Back](#)
[Close](#)
[Full Screen / Esc](#)
[Printer-friendly Version](#)
[Interactive Discussion](#)


High resolution land surface fluxes from satellite data (HOLAPS v1.0)

A. Loew et al.

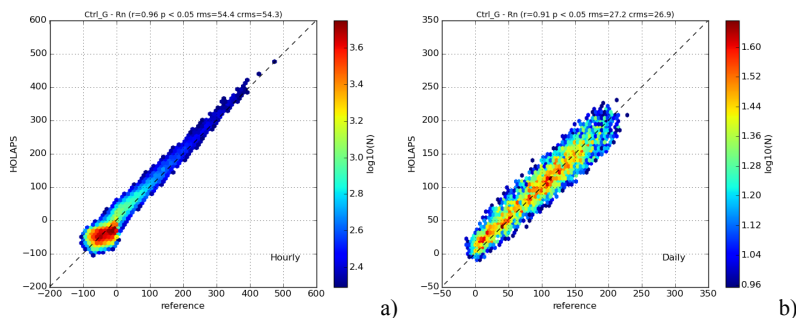


Figure 4. Comparison of surface net radiation flux (R_N) between FLUXNET measurements and HOLAPS estimates for **(a)** hourly and **(b)** daily timescales. Colors indicate the frequency of occurrence of values (data density).

[Title Page](#)[Abstract](#)[Introduction](#)[Conclusions](#)[References](#)[Tables](#)[Figures](#)[◀](#)[▶](#)[◀](#)[▶](#)[Back](#)[Close](#)[Full Screen / Esc](#)[Printer-friendly Version](#)[Interactive Discussion](#)

High resolution land surface fluxes from satellite data (HOLAPS v1.0)

A. Loew et al.

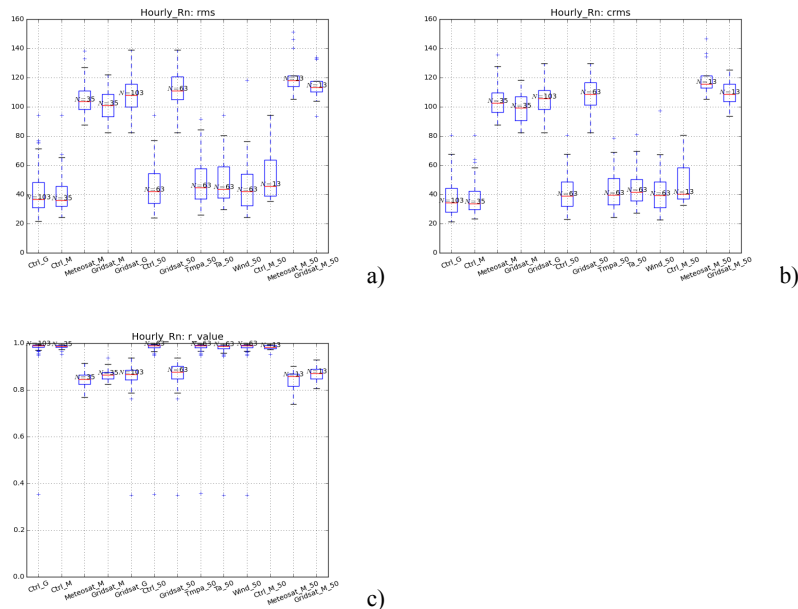


Figure 5. Boxplots of validation statistics for surface net radiation (R_N) for hourly data and all experiments investigated: **(a)** RMSD, **(b)** cRMSD, **(c)** correlation coefficient. The box corresponds to the inner-quartile range of the data and the red line indicates the median value. Numbers indicate number of model years for each experiment.

Title Page

Abstract

Introduction

Conclusions

References

Tables

Figures

◀

▶

◀

▶

Back

Close

Full Screen / Esc

Printer-friendly Version

Interactive Discussion



High resolution land surface fluxes from satellite data (HOLAPS v1.0)

A. Loew et al.

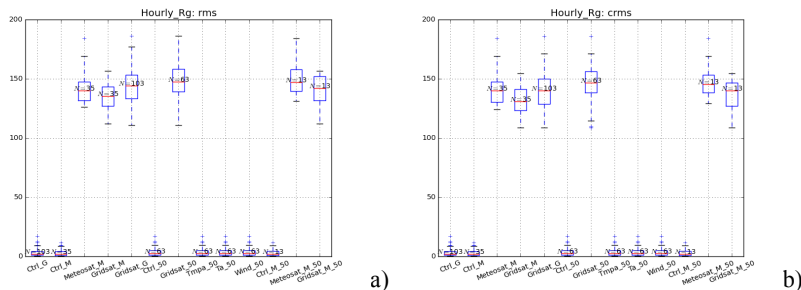


Figure 6. Boxplots of (a) RMSD and (b) cRMSD for hourly surface solar radiation flux (Rg).

Title Page	
Abstract	Introduction
Conclusions	References
Tables	Figures
◀	▶
◀	▶
Back	Close
Full Screen / Esc	
Printer-friendly Version	
Interactive Discussion	



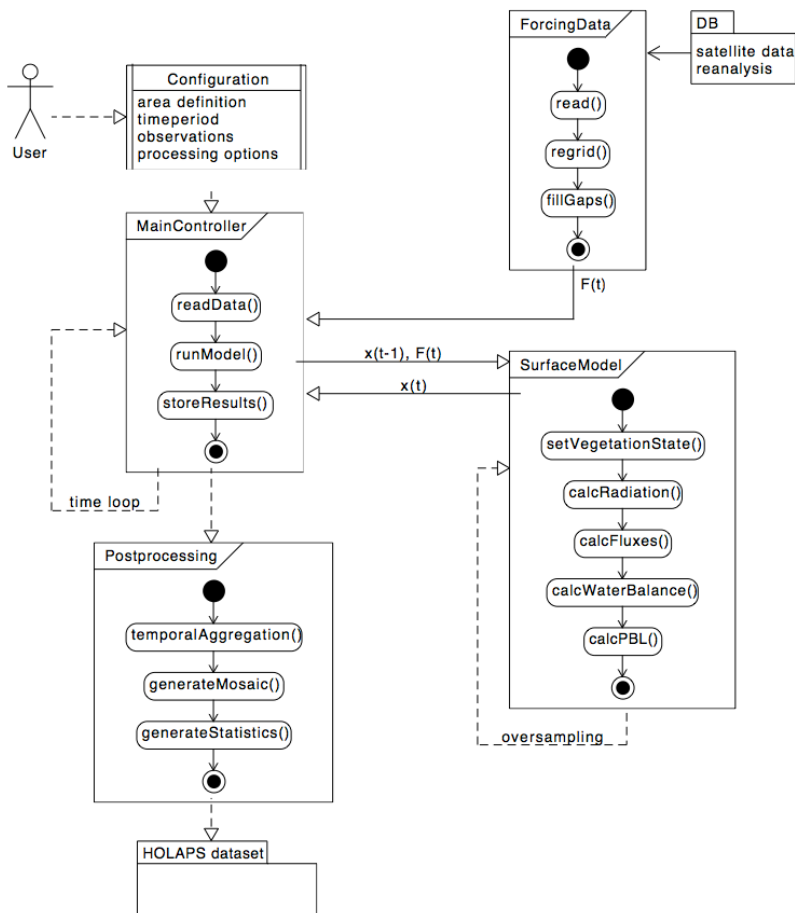


Figure B1. HOLAPS runtime environment.

High resolution land surface fluxes from satellite data (HOLAPS v1.0)

A. Loew et al.

Title Page

Abstract Introduction

Conclusions References

Tables Figures

⏪ ⏩

◀ ▶

Back Close

Full Screen / Esc

Printer-friendly Version

Interactive Discussion



High resolution land surface fluxes from satellite data (HOLAPS v1.0)

A. Loew et al.

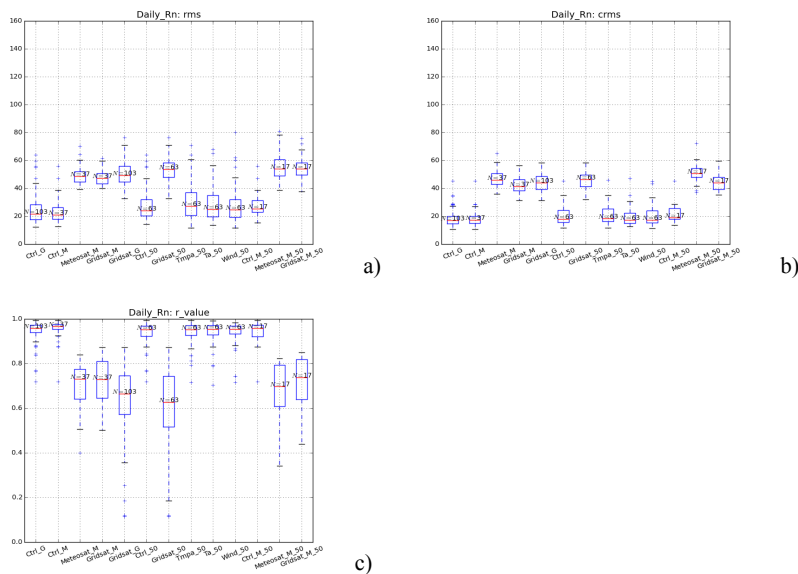


Figure D1. Similar error statistic for R_N like Fig. 4 but for daily timescales: **(a)** RMSD, **(b)** cRMSD, **(c)** correlation coefficient.

Title Page

Abstract

Introduction

Conclusions

References

Tables

Figures



Back

Close

Full Screen / Esc

Printer-friendly Version

Interactive Discussion



High resolution land surface fluxes from satellite data (HOLAPS v1.0)

A. Loew et al.

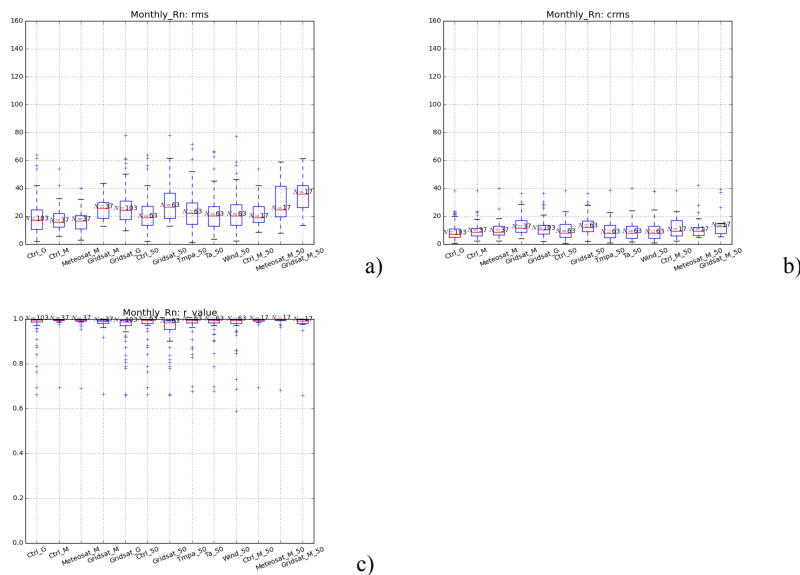


Figure D2. Similar error statistic for R_N like Fig. 4 but for monthly timescales: (a) RMSD, (b) cRMSD, (c) correlation coefficient

Title Page

Abstract

Introduction

Conclusions

References

Tables

Figures



Back

Close

Full Screen / Esc

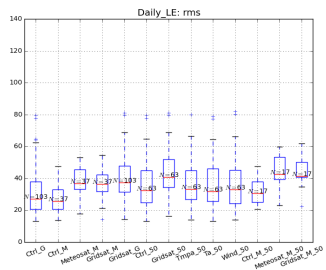
Printer-friendly Version

Interactive Discussion

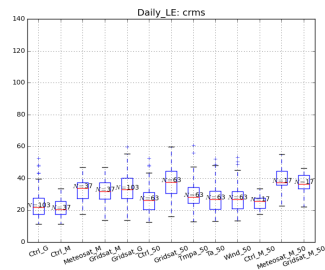


High resolution land surface fluxes from satellite data (HOLAPS v1.0)

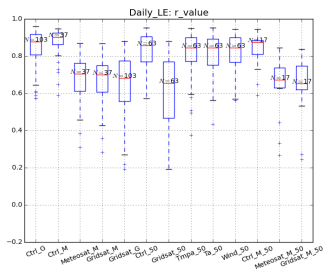
A. Loew et al.



a)



b)



c)

Figure D3. Similar error statistic for LE like in Fig. 8 but for daily values: **(a)** RMSD, **(b)** cRMSD, **(c)** correlation coefficient.

Title Page

Abstract

Introduction

Conclusions

References

Tables

Figures



Back

Close

Full Screen / Esc

Printer-friendly Version

Interactive Discussion



High resolution land surface fluxes from satellite data (HOLAPS v1.0)

A. Loew et al.

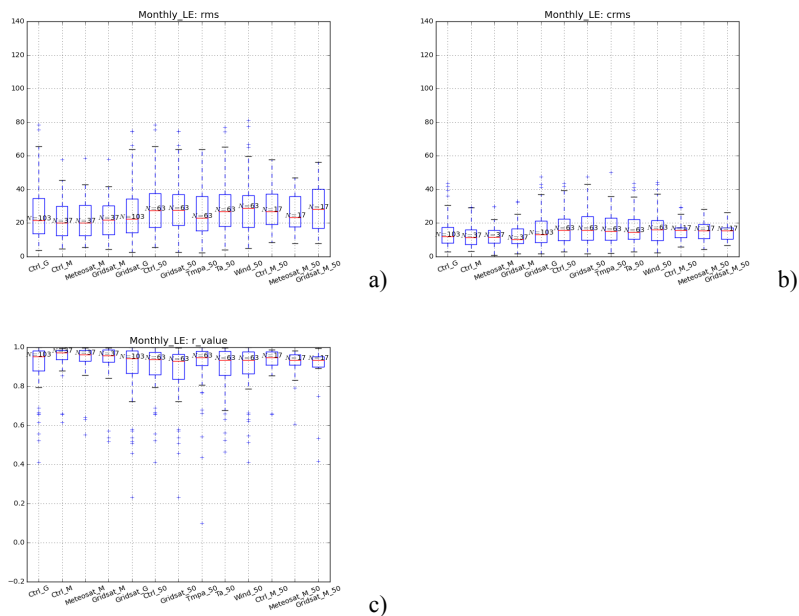


Figure D4. Similar error statistic for LE like in Fig. 8 but for monthly values: **(a)** RMSD, **(b)** cRMSD, **(c)** correlation coefficient.

Title Page

Abstract Introduction

Conclusions References

Tables Figures

⏪ ⏩

◀ ▶

Back Close

Full Screen / Esc

Printer-friendly Version

Interactive Discussion

